

## Electronic Supplementary Information

### Tunable Sn Structures in Porosity-Controlled Carbon

### Nanofibers for All-Solid-State Lithium-Ion Battery Anodes

*Dae-Hyun Nam,<sup>‡a</sup> Ji Woo Kim,<sup>‡b,d</sup> Ji-Hoon Lee,<sup>a</sup> So-Yeon Lee,<sup>a</sup> Hae-A-Seul Shin,<sup>a</sup> Se-Hee Lee,<sup>\*b</sup> and Young-Chang Joo<sup>\*a,c</sup>*

<sup>a</sup> Department of Materials Science and Engineering, Seoul National University, 1 Gwanak-ro, Gwanak-gu, Seoul 151-744, Republic of Korea

<sup>b</sup> Department of Mechanical Engineering, University of Colorado at Boulder, 427 UCB, Boulder, CO 80309, USA

<sup>c</sup> Research Institute of Advanced Materials (RIAM), Seoul National University, 1 Gwanak-ro, Gwanak-gu, Seoul 151-742, Republic of Korea

<sup>d</sup> Battery R&D Division, LG Chem. Ltd, Research Park, 188 Munji-ro, Yuseong-gu, Daejeon 305-738, Republic of Korea

\* Corresponding author, E-mail: [ycjoo@snu.ac.kr](mailto:ycjoo@snu.ac.kr), [sehee.lee@colorado.edu](mailto:sehee.lee@colorado.edu)

## 1. Thermal decomposition process of SnAc + PAN nanofibers

To fabricate Sn/C nanofibers, electrospun SnAc + PAN nanofibers need calcination, which is related with the thermal decomposition of SnAc and PAN. Based on the ambient conditions, they are categorized into combustion and pyrolysis. To determine the thermal decomposition of SnAc + PAN nanofibers, thermogravimetric analysis (TGA) and differential scanning calorimetry (DSC) were carried out in air and N<sub>2</sub> gas at a scan rate of 3 °C/min (Figure S6). In TGA, the air condition showed a 51.59 % weight decrease from room temperature to 700 °C. In contrast, the N<sub>2</sub> gas (inert) condition showed a 38.50 % weight decrease. This result can be explained by the difference between oxidation-based combustion and reduction-based pyrolysis. In the case of air (Figure S6a), SnAc forms tin dioxide (SnO<sub>2</sub>) *via* Sn oxidation, and PAN decomposes into gaseous products, such as CO<sub>2</sub> and H<sub>2</sub>O. In the temperature range from 100 °C, the weight percent started to decrease due to dehydration. In DSC, there existed an exothermic peak at approximately 250~300 °C, which shows cyclization of the nitrile group in PAN and decomposition of the acetate precursor.<sup>1,2</sup> The next exothermic peak at approximately 450 °C indicates the decomposition of the polymer matrix *via* combustion.<sup>1,3</sup> However, in the case of N<sub>2</sub> (Figure S6b), pure Sn phase can be formed *via* the reduction of SnAc. The pyrolysis products of PAN include not only gaseous products but also residual C with low molecular weight (M<sub>w</sub>) hydrocarbons. There also existed an exothermal peak at approximately 270 °C which indicates cyclization of PAN. When comparing the amount of heat in DSC, it can be determined that cyclization proceeds more vigorously in air.

Through Fourier transform infrared spectroscopy (FT-IR), the effect of stabilization on the formation of Sn/C nanofibers was investigated (Figure S7). FT-IR proceeded in the nanofibers after electrospinning, 200, 250 °C 1 h stabilization, and 700 °C 5 h calcination. In the electrospun nanofibers, peaks at 2940 and 1450 cm<sup>-1</sup> showed C-H stretching and bending, and the peak at 2240 cm<sup>-1</sup> showed C≡N stretching. However, after stabilization, these peaks started

to disappear and peaks appeared at  $1371\text{ cm}^{-1}$  (C-N bond) and  $1595\text{ cm}^{-1}$  (C-N, C-C stretching), which shows the formation of cyclized hexagonal rings.<sup>4</sup> As the stabilization temperature increased, these peak changes became clear at  $250\text{ }^{\circ}\text{C}$ . Finally, after  $700\text{ }^{\circ}\text{C}$  calcination, arrays of ring structures were formed, which was revealed by the peaks at  $1250\text{ cm}^{-1}$  (C-C bond). Although the ArNFs and HVNFs without stabilization showed N1s peak in the X-ray photoelectron spectroscopy (XPS), there was no N1s peak at approximately  $400\text{ eV}$  in the SANFs (Figure S9).

## 2. Electrochemical properties of Sn/C nanofibers according to the structures

Figure S10 shows the differential charge/discharge profiles ( $0.01 - 1.5\text{ V vs. Li/Li}^+$ ) of ArNFs after Ar calcination and HVNFs after HV calcination. The general peak shapes and displacement of them was correlated with that of pure Sn.<sup>5</sup> Considering the clear peaks with higher  $dQ/dV$  intensities for the ArNFs, the lithiation/delithiation reaction in the ArNFs proceeded faster than in the HVNFs. Nevertheless, the peak displacements were similar in both of them. After the 1<sup>st</sup> cycle, there was a negligible change in the profiles. In the reduction peaks for lithiation ( $0.45$  and  $0.67\text{ V}$ ), there was a peak shift after the 1<sup>st</sup> cycle due to the irreversible reactions related to SEI formation. The peaks from  $0.01$  to  $0.42\text{ V}$  disappeared after 1<sup>st</sup> cycle. The lack of peaks at  $1.05$  and  $1.55\text{ V}$  indicates that Sn is well covered by the outer C matrix, which can be seen in the TEM images of the ArNFs and HVNFs in Figure 1.<sup>6</sup> Based on the oxidation peaks ( $0.43$ ,  $0.56$ ,  $0.70$ , and  $0.78\text{ V}$ ), delithiation from  $\text{Li}_x\text{Sn}$  proceeds and the peak displacements agree with the literatures.<sup>5,6</sup> Compared with the charge/discharge profiles in Figure 5, they showed similarities between length of plateaus and intensity of peaks. As the voltage increased, Li was extracted from the Li-Sn alloy. Also, in Figure S10, the favorable phase of  $\text{Li}_{0.7}\text{Sn}$  was revealed more clearly. There was no change in the peaks according to the cycles, which implies good cyclability of the Sn/C nanofibers as active materials.

## REFERENCES

- 1 S. Y. Gu, J. Ren and Q. L. Wu, *Synthetic Met.*, 2005, **155**, 157–161.
- 2 P. S. Patil, R. K. Kawar, S. B. Sadale and P. S. Chigare, *Thin Solid Films*, 2003, **437**, 34–44.
- 3 N. Grassie and R. McGuchan, *Eur. Polym. J.*, 1971, **7**, 1357–1371.
- 4 I. Shimada, T. Takahagi, M. Fukuhara, K. Morita and A. Ishitani, *J. Polym. Sci. Pol. Chem.*, 1986, **24**, 1989–1995.
- 5 I. A. Courtney and J. R. Dahn, *J. Electrochem. Soc.*, 1997, **144**, 2045–2052.
- 6 Y. S. Jung, K. T. Lee, J. H. Ryu, D. Im and S. M. Oh, *J. Electrochem. Soc.*, 2005, **152**, A1452–A1457.

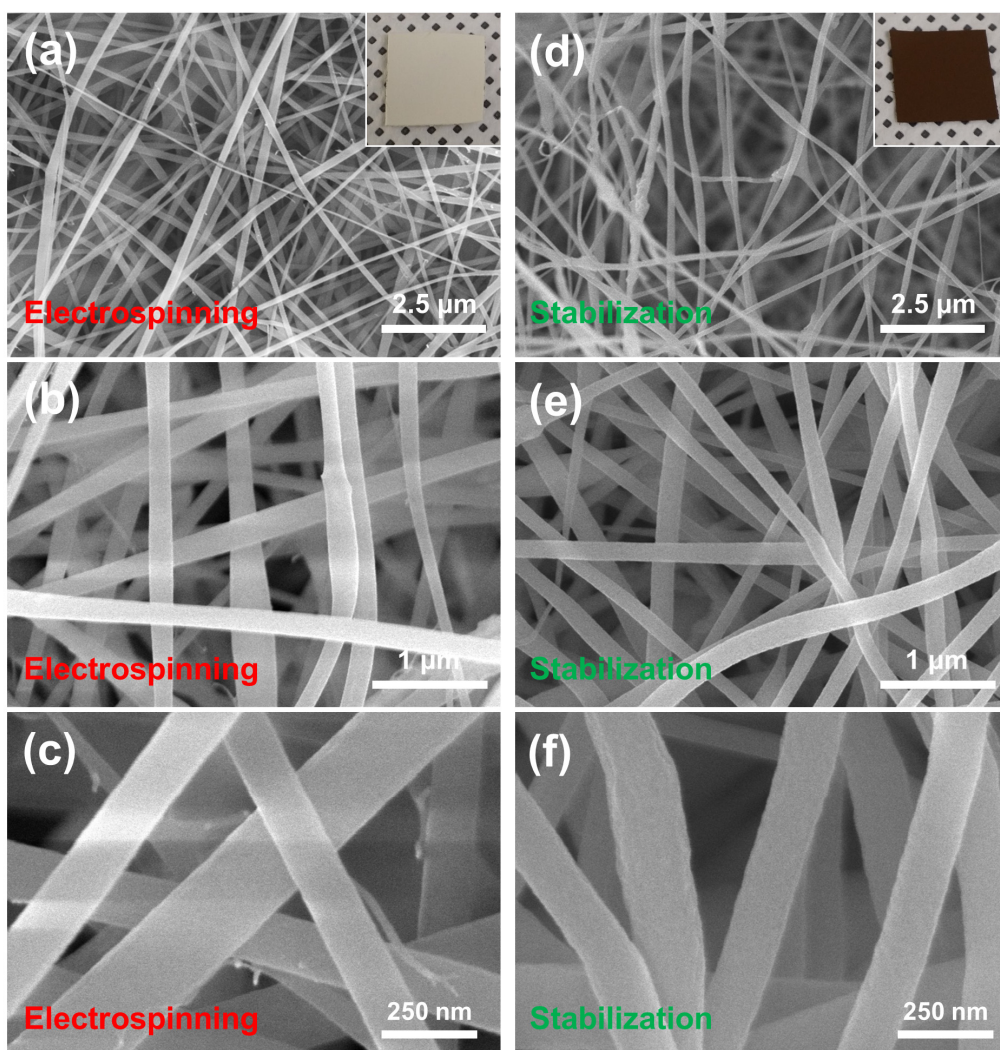


**Figure S1.** FE-SEM images with magnification and specimen photo images of nanofibers after (a-c) electrospinning (white) of SnAc + PAN and (d-f) stabilization (brown) at the condition of 250 °C, 1h in air. After stabilization, the surface of nanofibers become harsh. There is no abrupt structural change such as Sn agglomerates formation after stabilization.

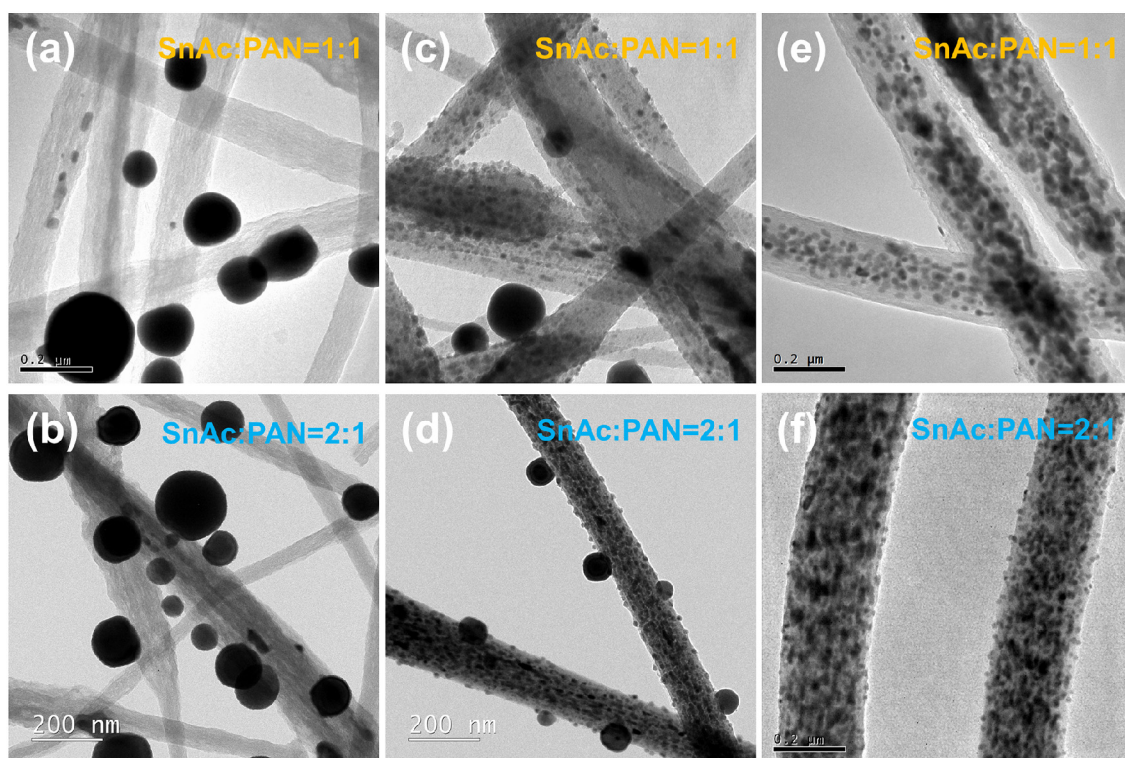


**Figure S2.** TEM images of Sn/C nanofibers according to the mass ratio between SnAc and PAN, calcination conditions. (a,b) SA calcination, (c,d) HV calcination, (e,f) Ar calcination. The formation tendency of Sn structure is similar with the 1:1 and 2:1 mass ratio. The difference of them is the amount of Sn in C nanofibers.

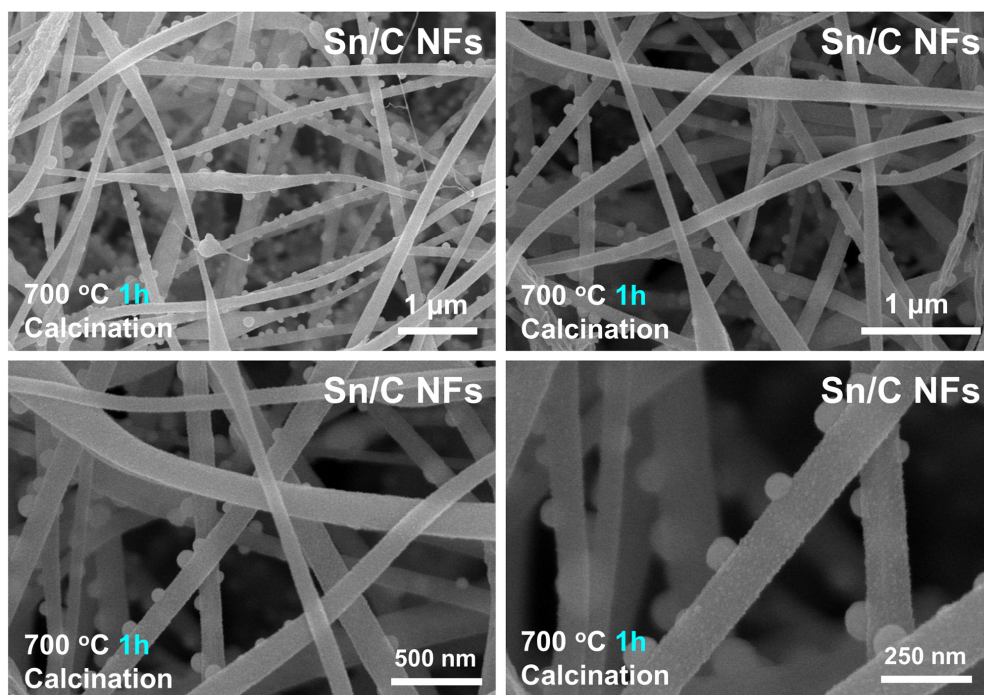


**Figure S3.** FE-SEM images for the investigation about the structures of Sn/C nanofibers after 700 °C high vacuum ( $<10^{-5}$  Torr) calcination of 1h isothermal time with various magnifications. The structures are similar with 5h calcinations and it reveals that outward Sn diffusion proceeds during cooling.

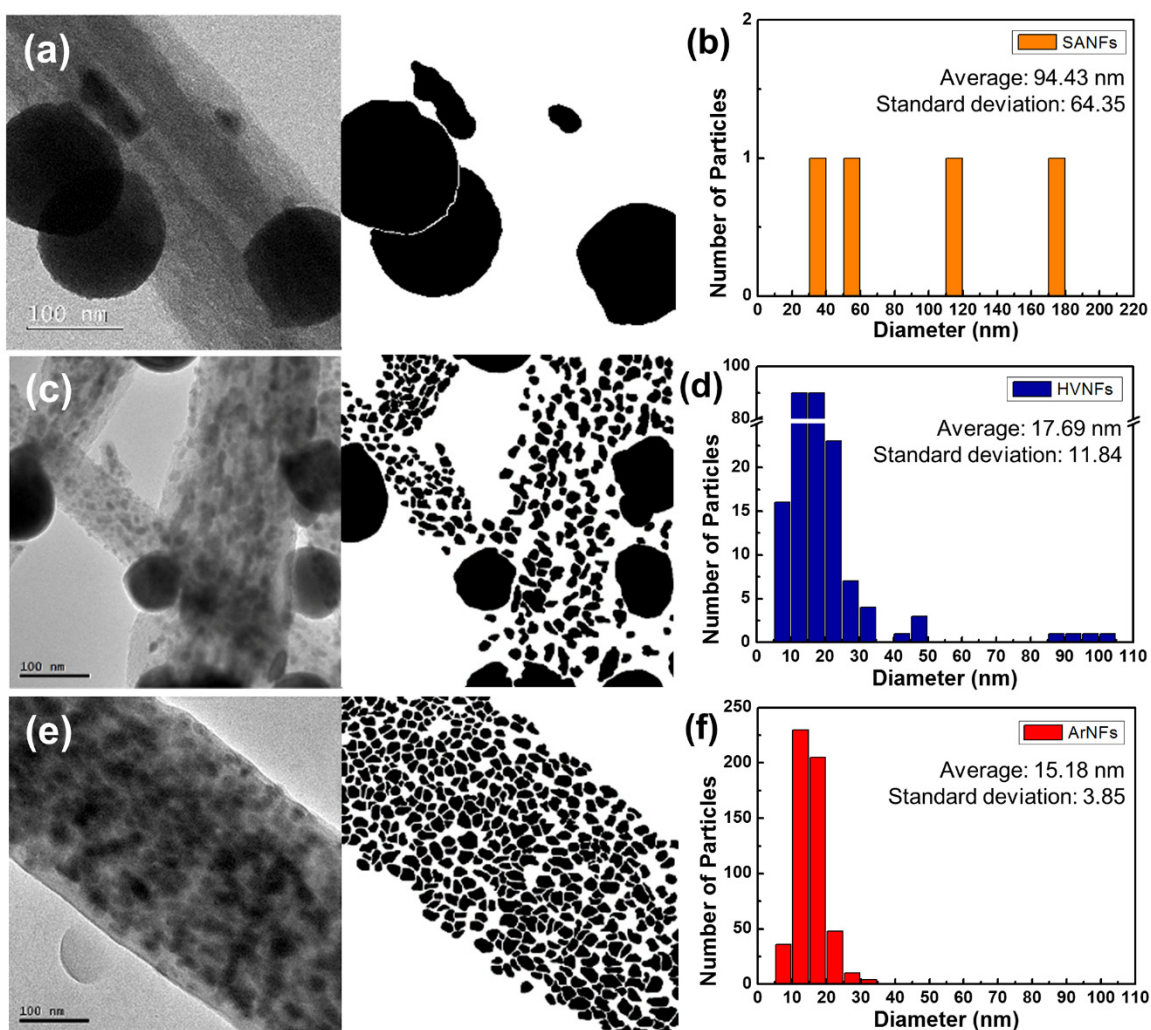


**Figure S4.** Transmission electron microscope (TEM) images, reproduced images for particle size and distribution analysis of the Sn/C nanofibers formed by (a,b) SA calcination, (c,d) HV calcination, and (e,f) Ar calcination. Sn particle distributions are represented by the histogram.

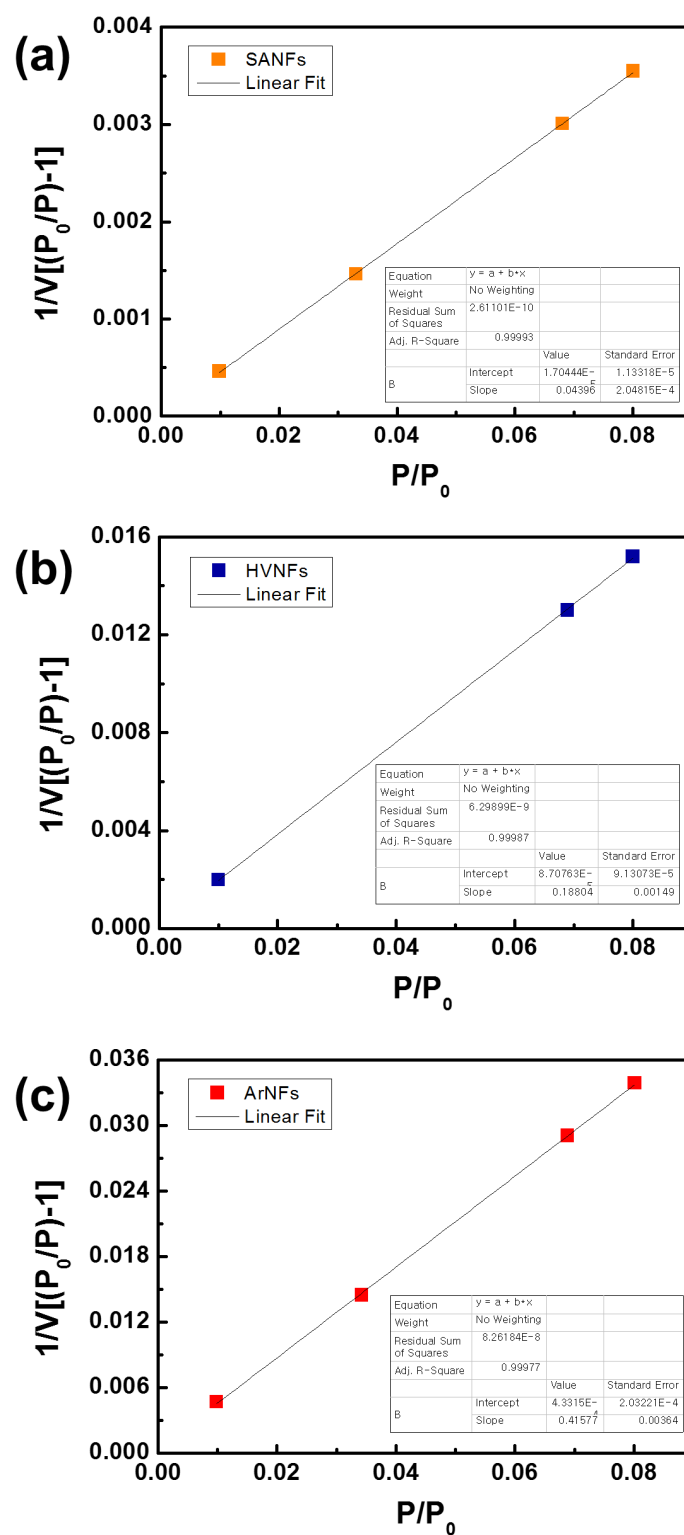


**Figure S5.** Fitting plot for investigating the Brunauer-Emmett-Teller (BET) surface area according to the relative pressure ( $P/P_0$ ). (a) SA calcination, (b) HV calcination, and (c) Ar calcination.

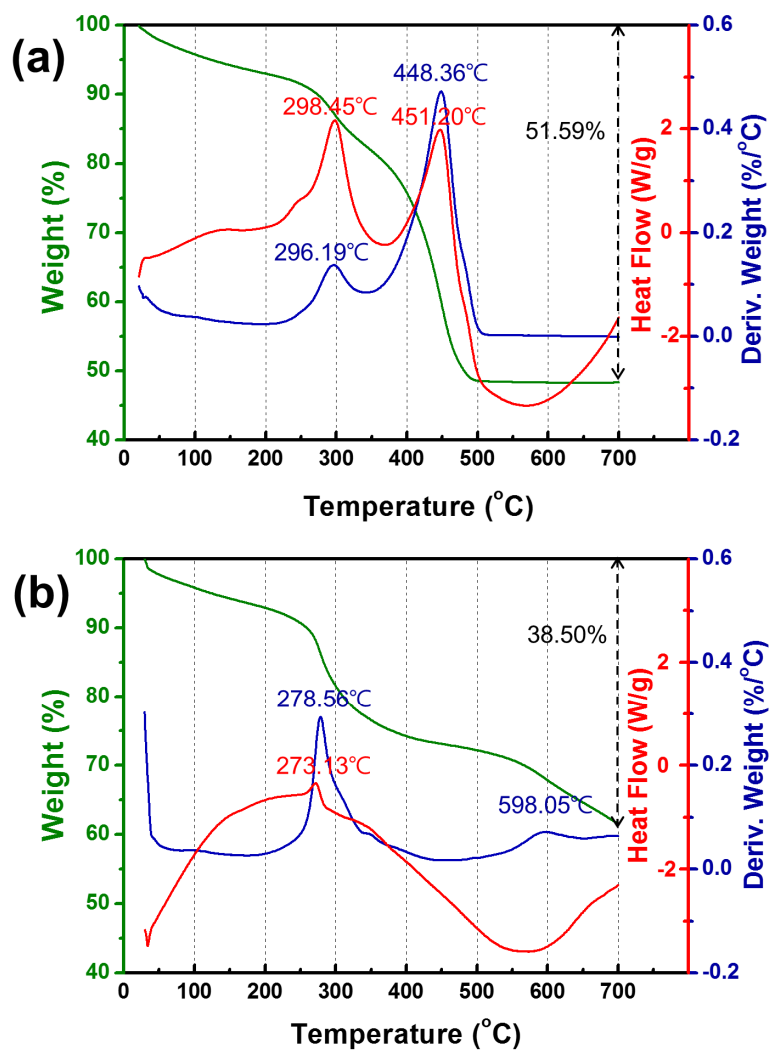


**Figure S6.** TGA and DSC of electrospun SnAc + PAN nanofibers to investigate the thermal decomposition process under (a) air and (b) N<sub>2</sub> gas flow in inert condition.

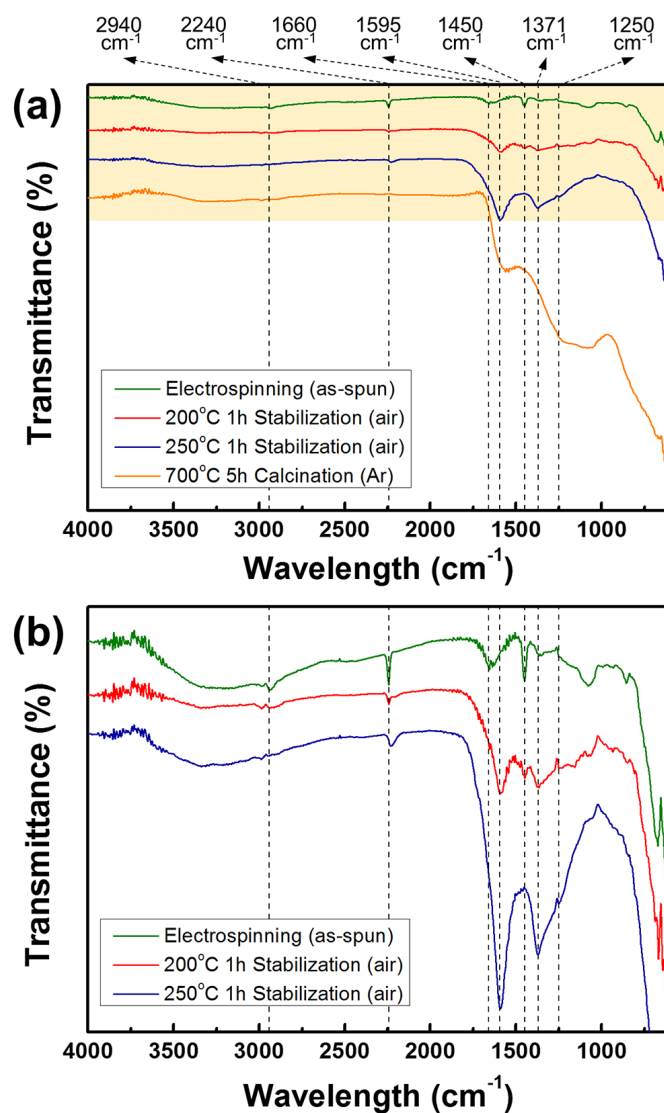


**Figure S7.** (a) FT-IR of Sn/C nanofibers from electrospinning to stabilization and calcination for investigating the thermal decomposition behavior of the SnAc and PAN. (b) Magnified range of transmittance in the FT-IR.

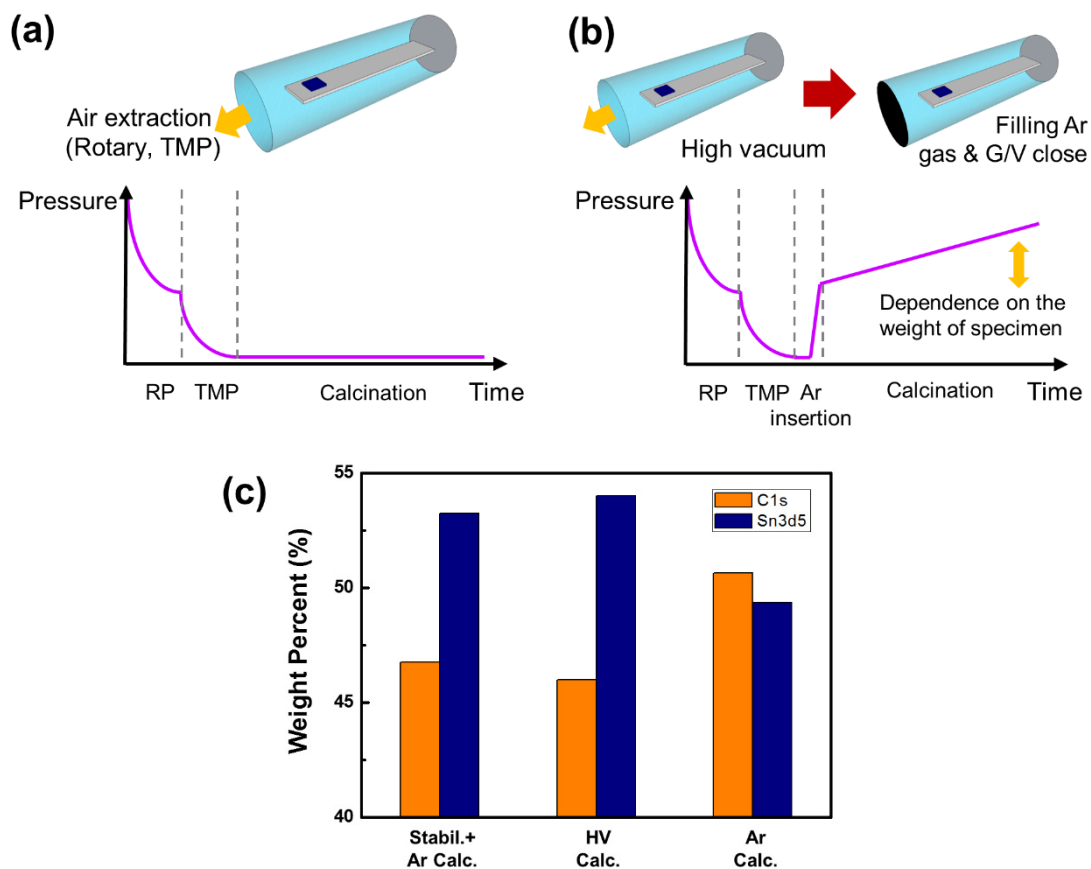


**Figure S8.** Calcination pressure and time profile schematics according to the tailoring methods of pressure equilibrium, such as (a) HV calcination and (b) Ar calcination. (c) XPS analysis for quantitative investigation of the weight percent ratio between C1s and Sn3d5 in the Sn/C nanofibers.

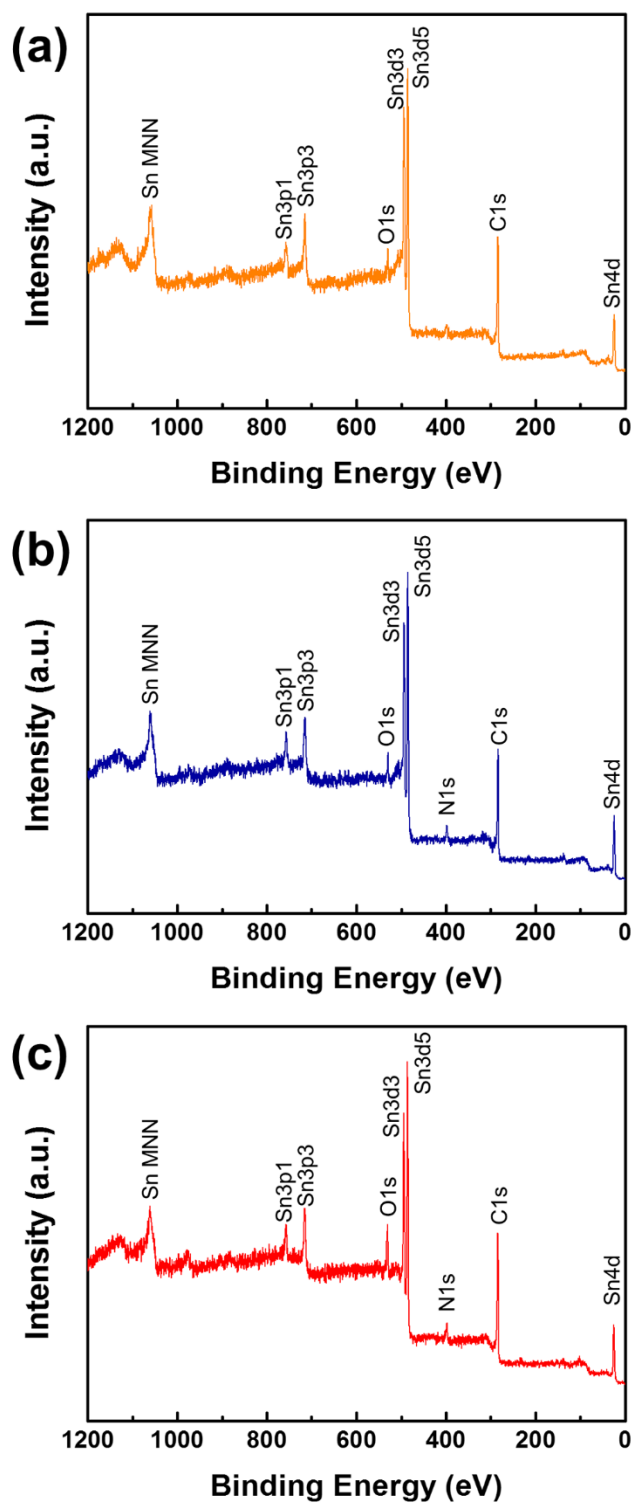


**Figure S9.** XPS spectra of the Sn/C nanofibers. (a) SA calcination, (b) HV calcination, and (c) Ar calcination.

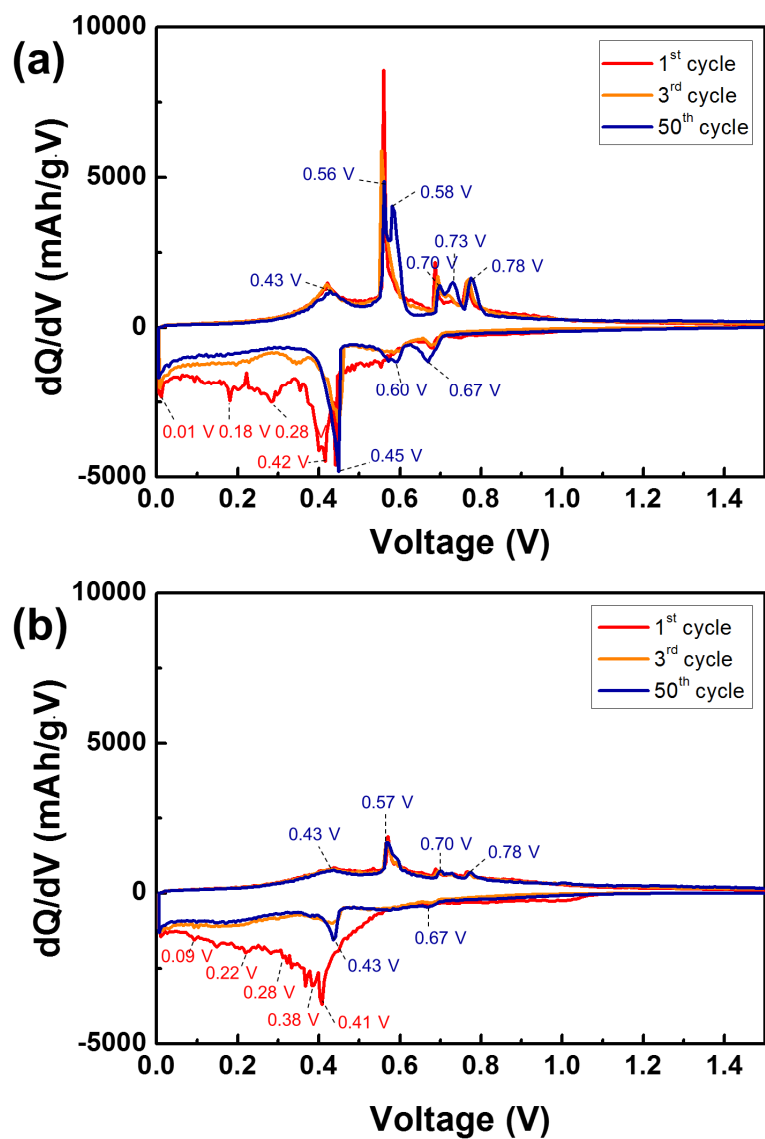


**Figure S10.** Differential charge and discharge profiles of (a) ArNFs and (b) HVNFs as the anodes in all-solid-state Li-ion cells from the 1<sup>st</sup> to the 50<sup>th</sup> cycle.